Journal Pre-proofs

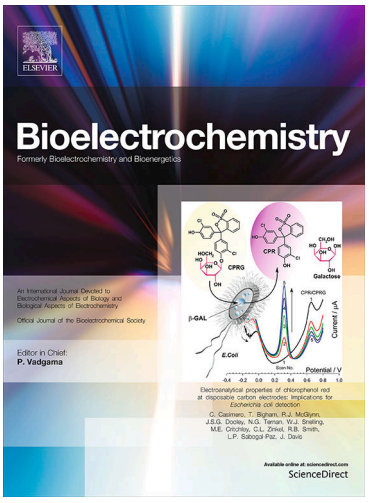

Electrodeposited Silver Amalgam Particles on Pyrolytic Graphite in (Spectro)Electrochemical Detection of 4-nitrophenol, DNA and Green Fluorescent Protein

Peter Sebest, Lukas Fojt, Veronika Ostatna, Miroslav Fojta, Ales Danhel

PII: S1567-5394(19)30409-8
DOI: https://doi.org/10.1016/j.bioelechem.2019.107436
Reference: BIOJEC 107436

To appear in: *Bioelectrochemistry*

Received Date: 19 September 2019
Revised Date: 26 November 2019
Accepted Date: 26 November 2019

Please cite this article as: P. Sebest, L. Fojt, V. Ostatna, M. Fojta, A. Danhel, Electrodeposited Silver Amalgam Particles on Pyrolytic Graphite in (Spectro)Electrochemical Detection of 4-nitrophenol, DNA and Green Fluorescent Protein, *Bioelectrochemistry* (2019), doi: https://doi.org/10.1016/j.bioelechem.2019.107436

Electrodeposited Silver Amalgam Particles on Pyrolytic Graphite in (Spectro)Electrochemical Detection of 4-nitrophenol, DNA and Green Fluorescent Protein

Peter Sebest[a], *Lukas Fojt*[a], *Veronika Ostatna*[a], *Miroslav Fojta*[a,b], *Ales Danhel*[a*]

[a] Institute of Biophysics of the Czech Academy of Sciences, Kralovopolska 135, CZ-61265 Brno, Czech Republic

[b] Central European Institute of Technology, Masaryk University, Kamenice 753/5, CZ-62500 Brno, Czech Republic

* e-mail: danhel@ibp.cz, tel. +420/541 517 143

Abstract

Catalytic properties and high adsorption affinity of nucleic acids and proteins to silver amalgam electrode surface make this kind of electrified interface perspective for bioanalytical and biomedical applications. For the first time, a basal-plane pyrolytic graphite electrode (bPGE) has been used as a substrate for electrodeposition of silver amalgam particles (AgAPs). Optimization of the resulting composition, surface morphology and electrochemical properties of the AgAPs was done by scanning electron microscopy with energy disperse X-ray spectroscopy, image processing software and voltammetric detection of electrochemically reducible model organic nitro compound, 4-nitrophenol. Spectro-electrochemical applicability of bPGE-AgAP has been demonstrated by electrolysis of 4-nitrophenol. Simultaneous UV-Vis-chronoamperometry provided information on the number of exchange electrons and the reduction rate constants. Preferential adsorption of the fluorescently labelled calf thymus DNA and the green fluorescent protein (GFP) on the surface of AgAPs was observed by fluorescence microscopy. In contrast to previously studied indium-tin oxide and vapour-deposited gold decorated by AgAPs, herein the presented bPGE-AgAP has provided sufficiently wide negative potential window allowing direct electroanalysis of non-labelled DNA and GFP using intrinsic electrochemical signals independently of the fluorescent labelling. The bPGE-AgAP can thus be expected to find application opportunities in protein electrochemistry, (bio)sensor development or *in-situ* spectro-electrochemical studies.

Keywords: DNA; Electrodeposition; 4-nitrophenol; Protein analysis; Silver amalgam particles; Spectroelectrochemistry

1. Introduction

The development of materials suitable for electrochemical, as well as spectroelectrochemical detection systems [1] is highly-valued for broad information content and system variability. Their applicability in direct detection of nucleic acids (NAs) and proteins or their constituents offers great potential for biophysical and biomedical research. Decentralized early-stage diagnoses of cancer or various genetic disorders could thus be controlled in the future. [2] Metal nanoparticles represent useful nanomaterial to develop modified electrodes applicable in specific detection of biomolecules, as well as in fabricating third-generation sensors with no need for a separate mediator. Nanoelectrode arrays offer high signal-to-background ratio and low detection limits and can thus be utilized in electroanalytical chemistry. [3] Up to now, direct label-free electrochemical analysis of NAs and proteins using their intrinsic redox signals has mainly been pursued on carbon or mercury-based working electrodes. [4,5] NAs and proteins offer chronopotentiometric "peak H" due to catalytic hydrogen evolution reaction (CHER) and/or intrinsic redox signals of selected nucleic bases or amino acids on mercury electrodes, respectively. The H peak's sensitivity towards NA's and protein structural changes could be envisaged in the development of novel detectors. [4–6] Unfortunately, increasing fear of mercury toxicity and its low mechanical stability hinder its broader application in developing biosensors and/or spectroelectrochemical devices.

Silver solid amalgam has been found to be a very promising electrode material since it exhibits similar electrochemical properties to mercury, lower toxicity, and strong mechanical stability. Silver solid amalgam electrodes (AgSAEs) have also been confirmed as an appropriate alternative to mercury electrodes in organic [7,8], as well as in DNA and protein electroanalysis. [4,5] In particular, AgSAEs have been successfully used to detect various synthetic oligonucleotides by alternating-current voltammetry [9] and cyclic voltammetry (CV) in the presence of copper ions [10] or enzymatically introduced redox labels. [11,12] Voltammetric analyses of purine bases, acid-treated DNA [13] together with DNA damage detection [14] and hybridization [15] have also been carried out on AgSAEs.

The most common preparation procedure of AgA electrodes is directly mixing silver powder and metallic mercury. This technique has been used to fabricate silver solid-, composite- and/or paste- amalgam electrodes. AgSAE was also modified using mercury film- or mercury meniscus- to emulate the smooth mercury surface. Porous flow through bioreactors and reference electrodes have been prepared from AgA. [16] While direct metal mixing is fairly easy and straightforward, the resulting heterogeneous electrode material has to be mechanically

polished or modified using mercury film or meniscus, then electrochemically activated and regenerated. In addition, it also lacks the possibility of automatized preparation and miniaturization down to the micrometer or nanometer scale. [17] We prepared needle-like AgA crystals by adding silver nitrate to metal mercury placed in water. [18] These working electrodes were successfully applied in batch voltammetric as well as in HPLC-amperometric systems. [19] Electrochemical silver(I) and mercury(II) ion co-reduction from their mixture on various conductive substrates allows simple and reproducible preparation of nanostructured, easily miniaturized [20] and also potentially photolithographicly patterned AgA surfaces. Thus, homogenous, sufficiently stable and mechanically robust AgA nano- and microparticles (AgAPs) with controllable constitution, size (less than 1 μm in diameter), distribution and surface coverage have already been electrodeposited on transparent indium-tin oxide (ITO) electrodes [20] and on vapour-deposited golden plate electrodes (vAuE) [21]. Our recent study has also demonstrated that they can exhibit plasmonic resonances in an extremely wide spectral window from ultraviolet up to mid-infrared wavelengths.[22] Unfortunately, beneficial transparency of ITO substrate is significantly limited by the applicable potential window (from +0.1 V to −0.7 V (vs. Ag/AgCl/3M KCl) in 0.2 M sodium acetate buffer (AcB) pH 5.0 or to −1.0 V (vs. Ag/AgCl/3M KCl) in 0.1 M KNO_3). Achievable potentials of ITO-AgAP are limited by anodic oxidation of AgAPs and cathodic reduction of In_2O_3 and SnO_2. The negative side of vAuE-AgAP's potential windows is limited by hydrogen evolution around −1.5 V (vs. Ag/AgCl/3M KCl) in 0.2 M AcB pH 5.0. Electrodeposited AgAPs thus broaden vAuE's potential window about 0.5 V to negative potentials, which allowed us to detect DNA labelled with osmium tetroxide-bipyridine complex. Golden support of vAuE was also found to be mechanically stable enough for repeated AgAP deposition and electrochemical anodic dissolution. [21] Unfortunately, no DNA or proteins intrinsic redox signals were observed on vAuE-AgAP or ITO-AgAP. Therefore, research of other supporting materials for AgAP's electrodeposition is essential to expand the bioelectrochemical application area.

The main aim of this work has been to study and optimize the process of AgAP electrodeposition on a basal-plane pyrolytic graphite electrode (bPGE), offering a remarkably wide applicable potential window (±2 V (vs. Ag/AgCl/3M KCl) in 0.2 M AcB pH 5.0 for the bare bPGE [23]). Applying the resulting nanostructured electrode in the voltammetric and spectroelectrochemical analysis was, systematically to ITO and vAuE, demonstrated on a model organic nitro-compound, 4-nitrophenol, an environmental pollutant [24] and the redox centre of a prospective DNA redox label. [25] Prospective utilization of bPGE-AgAP in

detecting NAs and proteins by cyclic voltammetry and highly sensitive constant current stripping chronopotentiometry has also been observed, respectively.

2. Experimental

2.1 Chemicals and reagents

Electroplating solution mixed from stock solution of 10 mM $AgNO_3$ (p.a. 99.8 %, Safina) and 10 mM $Hg(NO_3)_2$ in 0.1 M KNO_3 (p.a. >98 %, Fluka) was prepared by the same procedure as described in Ref. [20,21]. Metal alloy composition in the whole paper is attributed to the content of silver in terms of percentage weight ($w\%_{Ag}$). A 1 mM solution of 4-nitrophenol (4-NP, >99.0 %, Sigma-Aldrich) served as an electrochemical probe and typical reducible analyte. All 4-NP voltammetric studies were performed in 0.2 M AcB pH 5.0. A single-stranded oligodeoxyribonucleotide (ODN) 5´-CATCCATCACATCACTCCCAGTCCGCCCTAG-3´ (Generi Biotech) and a recombinant *E. coli* green fluorescent protein, (GFP, His-tag, Abcam) dissolved in PBS, pH 7.4 were used as model biomolecules (DNA and protein, resp.) to be detected on bPGE-AgAP.

Calf thymus DNA (for molecular biology, Sigma Aldrich) was dissolved to the resulting DNA concentration 20 ng μL^{-1} in deionized water and labelled with a dsDNA Broad Range Fluorescence Assay according to the technical note No. 143 (DeNovix). Other compounds were at least *p.a.* purity purchased from Sigma-Aldrich. All solutions were prepared from deionized water (18.2 MΩ cm, Purelab Option-Q, ELGA) and stored in a refrigerator at 4°C, if not stated otherwise.

2.2 Instruments and procedures

AgAP electrodeposition was performed by double-pulse chronoamperometry (DPCA) in a three-electrode setup composed of: i) a bPGE or edge-plane PGE (ePGE, both Momentive) working electrode, together with ii) a refillable miniature Ag/AgCl/3M KCl reference electrode (eDAQ) placed into the salt bridge composed of a heat shrink Teflon tube (Qualtek) enclosed by CoralPor® (BASi) filled by 0.1 M KNO_3 and iii) a glassy carbon rod auxiliary electrode (Metrohm-Autolab). The PGE with AgAPs was rinsed in 0.1 M $HClO_4$ and in deionized water immediately after the electrodeposition and prior to further electrochemical studies, in order to remove any remaining metal salt residues. Three consecutive cyclic voltammograms were also registered within the potential window ($E = \{-0.1; -1.2\}$ V) in the base electrolyte before each voltammetric measurement of 4-NP or DNA; CPS analysis of the protein did not require such preconditioning.

Further electrochemical measurements (with Ag(I), Hg(II), 4-NP and DNA) were carried out by Autolab PGStat128N potentiostat operated by Nova software Ver. 2.13 (both Metrohm-Autolab), while chronopotentiometric GFP stripping was performed by Autolab 302N (Metrohm-Autolab) with GPES as the operating software. The potentiostat was connected with VA Stand 663 in a three-electrode setup including: bPGE or bPGE-AgAP as the working electrode, Ag/AgCl/3M KCl as the reference electrode and a platinum rod as the counter electrode (both Metrohm-Autolab). All potentials are reported with respect to the Ag/AgCl/3M KCl reference electrode, if not stated otherwise. Cyclic voltammograms were registered from 0.0 V to −2.2 V by staircase cyclic voltammetry using scan rate 0.10 V s^{-1} and step 0.024 V. Oxygen was removed from all investigated solutions by letting a stream of argon (5.0 grade, SIAD) saturated with water vapour to pass through them for 5 min before starting the experiments. Adsorptive transfer stripping (AdTS) voltammetry was done by adsorption of the ODN on bPGE-AgAP during 4 min from 4 µL aliquot of 100 µg mL^{-1} ODN in 0.3 M NaCl, which was subsequently dipped into the deionized water and then in 0.3 M AFP buffer pH 6.9, where voltammetric experiments were finally done using scan rate 1.0 V s^{-1}. Chronopotentiometric stripping (CPS) was performed under air. All measurements were carried out at room temperature (25°C).

Surface morphology was analysed using a scanning electron microscope (SEM, Verios 460L, FEI) including energy-disperse X-ray spectrometer (EDS, EDAX SSD Octane Super) allowing determination of AgAPs composition using acceleration voltage 6.0 kV, beam current 0.80 nA and magnification: 200×, 600× 1200×, 4 500×, 10 000× and/or 20 000×. Average particle size, distribution and surface density/coverage was determined by freeware ImageJ.[26]

The spectroelectrochemical cell was assembled according to Danhel et al. [20] in a 1-cm quartz cuvette. Linear scan voltammetry (LSV) together with potentiostatic chronoamperometry were controlled by potentiostat PalmSens 3 using PSTrace 5 software (both PalmSens). The transmission spectra were acquired in the wavelength region between 230 and 450 nm in 10 s intervals by Specord 210 Plus using software WinASPECT Plus Ver. 4.2.0.0 (both Jena).

Inverted fluorescence microscope (IX83, Olympus) with LED light source (pA-300^{White}, CoolLED), CMOS camera (ORCA-Flash 4.0 LT, Hamamatsu) and 60× objective (UPLFLN, N.A. 0.90, W.D. 0.2, Olympus) was used for imaging of the bPGE and ePGE surfaces with electrodeposited AgAP and adsorbed DNA (60 s, 20 µg mL^{-1} of DNA in 0.3 M NaCl) or GFP (60 s, 5 µM of GFP in 0.05 M PhB pH 7.0 and 0.02 M NaCl). Fluorescence of the labelled DNA was registered in the same microscope using 560 nm excitation and 635 nm emission

wavelengths. 488 nm excitation and 509 nm emission wavelengths were used for GFP. The model ODN and protein were analysed using an adsorptive transfer stripping (AdTS) technique. The analyte was accumulated on the electrode surface from 5 µL aliquots (10 µM ODN in 0.3 M NaCl, 3 µM GFP) for 5 minutes, followed by washing the electrode in deionized water and placing it into the electrochemical cell. ODN's CV measurements were performed in 0.3 M ammonium formate with 0.05 M sodium phosphate (AFP) buffer, pH 6.9, as the background electrolyte. The CV parameters were set as follows: initial potential 0.0 V, switching potential −2.0 V, final potential 0.0 V, scan rate 1.0 V s^{-1}. GFP was adsorbed for 300 s at OCP from PBS pH 7.4 and analysed in 0.05 M sodium phosphate, pH 7, by chronopotentiometry with stripping current I_{str} −300 µA (if not stated otherwise).

3. Results and Discussion

3.1 Electrochemical behaviour of Ag(I) and Hg(II) at bPGE

In principle, AgAPs may be electrodeposited from proper precursors (*e.g.* nitrates, perchlorates or acetates) on a conductive substrate with a suitable potential window. Precursors $AgNO_3$ and $Hg(NO_3)_2$ were chosen with respect to their good solubility in aqueous solutions, mutual tolerance towards precipitation, stability, and availability. Knowledge of the selected precursors' voltammetric behaviour on the selected substrate helps to determine intervals of nucleation and growth deposition potentials for the herein utilized DPCA (Chap. 3.2). Registered cyclic voltammograms of individual Ag(I) and Hg(II) ions and their mixture (Ag(I)/Hg(II), 10 mM, 30.6 $w\%_{Ag}$) on bPGE (Figure 1) showed cathodic peaks due to Hg(II) and Ag(I) reduction around +0.215 V. They are followed by two cathodic waves related to the reduction of H^+ and K^+ on electrodeposited metallic mercury or AgAPs at potentials more negative than −1.0 V (Figure 1b and 1d, respectively). Lower hydrogen overpotential of silver caused significantly high hydrogen reduction at potentials more negative than −0.70 V (Figure 1c). Further current rush can be attributed to hydrogen evolution on the underlying bPGE. Anodic peaks at +0.695 V correspond to the oxidation of deposited metals. Ag's anodic dissolution is characteristic by three current maxima at +0.80 V, +0.92 V and +1.13 V. These peaks apparently correspond to oxidation of different sizes of silver particles [27] and/or various forms of Ag(I) and Ag(III) oxide emergence.[28] Since no significant differences were observed in the reduction of the metals in or without the presence of oxygen, AgAP depositions were carried out in the presence of oxygen for simplicity. The shapes of cyclic voltammograms of Ag(I)/Hg(II) mixture (30.6 $w\%_{Ag}$; Figure 1, green curve) were similar to that of only Hg(II) in the first scan, showing one cathodic peak. In the second scan, the latter peak was shifted by

about 0.150 V towards more positive potentials due to mercury's more negative nucleation potential than silver's. About 60 mV more positive oxidation peak of AgAP (than Hg) documents mutual chemical stabilization. When both metal ions are present, metallic mercury droplets are formed on the electrode surface first, and then Ag(I) is reduced on them by electrochemical and/or by a chemical process, depending on the applied potential. Ag(I) chemical reduction proceeds to the exclusion of metal mercury oxidation at potentials more positive than +0.2 V. The electrochemical process prevails over the chemical one with applied potential more negative than +0.2 V. Decreasing the potential to more negative values makes the electrochemical process faster, but with a detrimental effect on AgAP's crystallinity. This is in agreement with our previous data [20] and with other studies of the silver amalgam nucleation process.[29] From registered voltammograms, final nucleation potential intervals (E_1 = {−1.0;−2.0}V) and growth potential (E_2 = {+0.4;−0.5}V) could be selected for their further optimization and for successful of AgAP electrodeposition on the bPGE by DPCA.[30]

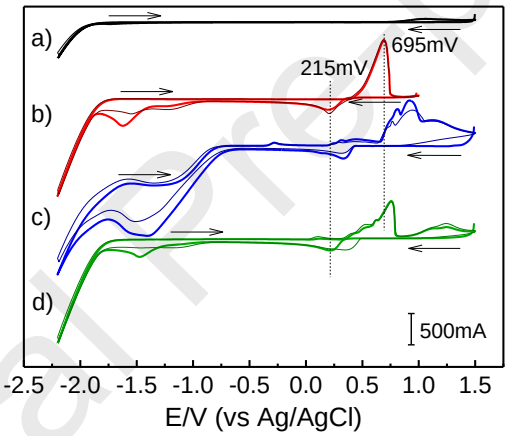

Figure 1. Two consecutive cyclic voltammograms (1st bold, 2nd light) of: 10 mM Hg(II) (b), 10 mM Ag(I) (c), and 10 mM Ag(I)+Hg(II) (30.6 $w\%_{Ag}$) (d), all in 0.1 M KNO_3 at bPGE (a).

3.2 Electrodeposition of silver amalgam

AgAPs' composition, crystallinity, surface density, and size may be controlled by proper selection of metals' ratio together with their total concentration in the deposition solution and individual DPCA parameters (nucleation and growth potentials and times). The nucleation potential influences the number of nucleation centres related to AgAPs' final density. The few tens of milliseconds' nucleation time have only a negligible influence on the AgAPs' surface morphology. The growth potential considerably influences AgAPs' crystallinity and morphology. The growth time mainly influences their particles' size. [29] First, the deposition solution's composition, the Ag(I)/Hg(II) ratio, was observed using selected DPCA parameters.

The individual DPCA parameters were later successively optimized at the selected Ag(I)/Hg(II) ratio.

Influence of solution constitution. To study the influence of the solution properties on the composition of the resulting AgAPs, we selected the following DPCA parameters: Nucleation potential (E_1) −1.25 V applied for nucleation time (t_1) 50 ms, followed by growth potential (E_2) +0.4 V lasting for growth time (t_2) 1 min. The relative Ag(I) and Hg(II) content was then adjusted to various percentages while keeping the net [Ag(I) + Hg(II)] concentration constant and equal to 10 mM. The representative SEM images of the resulting sequence of electrodes are shown in Figure 2; the composition of the individual AgAPs was also studied by EDS (Supporting Information, Figure S1). In the extreme cases of 100 $w\%_{Hg}$ and 100 $w\%_{Ag}$, uniform droplets of electrodeposited mercury and silver particles of variable size were found on the electrodes, respectively. One would expect the content of electrochemically co-deposited metals in the AgAPs to be directly proportional to the content of the metals in the source solution (dash-dot lines in Figure S1). However, significant differences were observed between the range of 8.7 to 61.7 $w\%_{Ag}$ in the solution, which indicates the preferential formation of stable AgA forms. Following AgA crystal phases: γ (body-centered cubic, 29.0–32.5 $w\%_{Ag}$), β (hexagonal close-packed, 33–48 $w\%_{Ag}$) and α (face-centered cubic, >48 $w\%_{Ag}$) may be found on the substrates. [31] Electrodeposition from solutions of 15.2 to 39.7 $w\%_{Ag}$ resulted in forming AgAP with mutually comparable average composition 42±3 $w\%_{Ag}$, increasing particle surface density and decreasing the average particle size (for illustration compare Figure 2b, c, d, e). The number of the particles and resulting bPGE surface coverage also increased with an increasing Ag/Hg ratio in the solution. This trend also continued for solutions of 39.7, 50.0 and 61.7 $w\%_{Ag}$, while the average Ag content in AgAP increased from 43.7 to 49.0 and 56.1 $w\%_{Ag}$, respectively (Figure 2f, g, h).

The composition of the individual AgAPs together with the overall electrode surface morphology significantly influences the resulting bPGE-AgAP electrodes' electrochemical properties. From the electroanalytical point of view, AgA with about 40 $w\%_{Ag}$ offers the broadest potential window [32–34] and the strongest electrochemical responses towards a number of inorganic and organic compounds (as reviewed in Refs. [7,8,35]). Since the AgAP's composition only slightly varied around 42±3 $w\%_{Ag}$ for a broad range of Ag(I) content in the solution, the solution containing 30.6 $w\%_{Ag}$ (Figure 2e) was selected for further optimization of DPCA parameters in order to find a compromise between the suitable electrochemical properties, particle size and surface coverage.

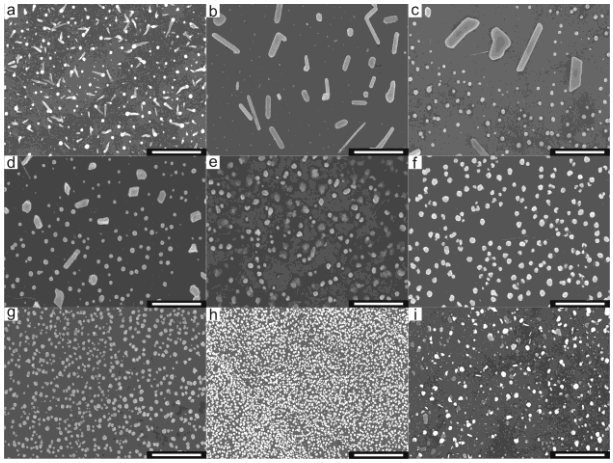

Figure 2. SEM images of AgAP electrodeposited on bPGE from a solution containing: 0 (a), 8.7 (b), 15.2 (c), 22.5 (d), 30.6 (e), 39.7 (f) 50.0 (g), 61.7 (h) and 100 $w\%_{Ag}$ (i), using DPCA. Magnification is 10 000×, all scale bars are 5 μm.

Influence of DPCA parameters on AgAP properties. Using the solution selected according to the analysis mentioned above, we will now discuss the influence of individual DPCA parameters on AgAP properties. The SEM images of the AgAPs electrodeposited on the bPGE using selected DPCA parameter combinations see in Figure S2. The resulting AgAP composition obtained from the EDS analysis, together with the particle size (determined as an average size of AgAPs in μm^2 calculated as a ratio between geometric surface area of AgAPs and their total number within the observed area) and the relative surface coverage (*RSC*, calculated as a ratio between geometric surface area of AgAPs and total surface area of bPGE-AgAP) are shown in Figure S3. In general, the composition of the AgAPs varied in an interval of 45±4 $w\%_{Ag}$ during DPCA parameter optimization (E_1, E_2, and t_2) in a solution of 10 mM Ag(I)/Hg(II) (30.6 $w\%_{Ag}$). This indicates the DPCA parameters only have a negligible influence on the AgAPs' composition and a constant deposition rate/efficiency of the metals on the bPGE. First, the nucleation potential (E_1) was optimized between −1.0 and −2.0 V, while the rest of the parameters were kept constant (t_1 50 ms, E_2 +0.4 V and t_2 60 s). The average electrodeposited AgAP size (Figure S3, red points) varied from 0.04 to 0.1 μm^2 (i.e., 220–360 nm in diameter). The minimum particle size together with the maximum *RSC* of 27 % was reached at E_1 −1.25 V (Figure S3, left panel). This potential was selected to further optimize E_2 and t_2. The amount of Ag in AgAPs decreased from 48 to 43 $w\%_{Ag}$ with decreasing E_2 from +0.5 to −0.5 V, while the RSC raised up to 47±2 % and particle size varied around 200±20 nm in diameter (Figure S3, central panel). Growth time t_2 had only a little impact on the AgAP composition (which varied between 42 and 49 $w\%_{Ag}$ for t_2 ranging), but significantly influenced

RSC, which raised from only 20 % to a maximum value of 67 % from 30 s to 5 min (Figure S3, right panel), respectively. Further increasing t_2 up to 10 min caused aggregation of individual AgAP and formation of a sponge-like AgA structure.

Here we showed that AgAPs may optionally be controlled by selecting suitable DPCA parameters in limited density, size and surface coverage. E_1 influences density and E_2 lasting t_2 affect the AgAP size with RSC. The obtained AgAP properties may still be improved by a different net concentration of the metals or content of Ag(I) in the mixture. Furthermore, the lower total concentration of the metals and/or additional capping reagents' presence (*e.g.* sodium citrate or cetyltrimethylammonium bromide) may lead to *e.g.* decrease in minimal particle size and/or increase in particle homogeneity.[36] This is in the scope of our further research. Optimal DPCA parameters for AgAP electrodeposition on the bPGE will be selected according to the coincidence of AgAP properties and 4-NP voltammetric response discussed below (Chapter 3.3).

bPGE-AgAP was found to be mechanically stable enough to persist common manipulation such as gentle washing, transfer between various solutions or storage on air during several months. Just in case of necessity, AgAPs may be partially wiped off from the bPGE surface by *e.g.* paper tissue. Thanks to the simple and fast preparation of AgAPs, AgAPs may be deposited just before its use. The preparation process also included a registration of cyclic voltammograms within the potential window in base electrolyte before each measurement. Application of negative potentials simply removes possible Ag oxidation products from the surface and secures repeatable measurements. Regarding the chemical stability of AgAPs, since metallic mercury and silver have very similar standard redox potentials, they are electrochemically oxidized practically simultaneously. Nevertheless, the metallic silver is stabilized by amalgamation in AgAPs and thus it is more stable towards oxidation than silver particles themselves. This has been shown by a corrosion study published in Ref. [21]. Higher oxidation stability of AgAPs facilitate its practical application in optical experiments, such as surface plasmon resonance, since silver has a very high activity of surface plasmons, but its simple oxidation hinders its broader applicability.

3.3 Voltammetry of 4-nitrophenol

Cyclic voltammetry of 4-NP on bPGE-AgAP. The DPCA parameter optimization for AgAP electrodeposition on bPGE was complemented by 4-NP voltammetric measurements using CV (Figure S4). The influence of the AgAPs' morphology on their electrochemical behaviour could thus be explored. Cyclic voltammograms of 4-NP were registered on a bare

bPGE and on bPGE-AgAPs electrodeposited from the different Ag(I) and Hg(II) content solutions. Low bPGE surface coverage by the AgAP using t_2 1 min gave rise to cathodic peaks (labelled p1 and p2) corresponding to the reduction of 4-NP on the AgAPs and the underlying bPGE, respectively (Figure S4). Prolonging t_2 to 5 min increased RSC, which resulted in suppressing p2 peak and increasing p1 and p3 peaks. The solution's constitution was optimized again with the t_2 5 min (Figure S5). Representative cyclic voltammograms of 4-NP acquired on a set of bPGE-AgAPs, prepared with various combinations of the selected DPCA parameters together with the evaluated peak potentials (E_p) and currents (I_p), are shown in Figure S6. The signal p2 still appeared on the samples with an AgAP composition within 0 to 22.5 w%Ag (w_{SOL}). Higher Ag(I) content in the solution, together with prolonging the deposition time to 5 min, lead to sufficient surface coverage and resulted in a well-developed and separated (from the p2 peak) cathodic p1 peak. In agreement with the well-established mechanism of 4-NP reduction [37], the p1 peak corresponded to four-electron reduction of the nitro group to a hydroxyamino group, which is then further reduced by another two electrons to an amino group and gave the p3 peak. [18] A solution concentration of 30.6 $w\%_{Ag}$ and DCPA parameters E_1 −1.25 V, t_1 50 ms, E_2 +0.4 V, and t_2 5 min were thus selected for further electrochemical analysis with respect to the small size and high AgAP RSC on the bPGE providing high, well-defined of 4-NP responses. Applicability of the bPGE-AgAPs to detect 4-NP by CV was investigated in more detail.

Determination of the electrode process. 4-NP CV peak heights were measured on a bPGE-AgAP as a function of the scan rate (in the range of 0.050 and 1.0 V s^{-1}) to determine whether the electrochemical reduction process is driven either by diffusion or adsorption. The p1 and p3 peak currents were found to linearly increase with the square root of the scan rate (Figure S7 and Table S1). This confirms that 4-NP's electrochemical reduction on the bPGE-AgAP is diffusion controlled. A significant increase in the p3 peak also gives evidence of this electrochemical process's enhancement by AgAPs. The analogical behaviour has already been observed on single crystal silver amalgam electrodes, where it was even more pronounced than on a hanging mercury drop electrode (HMDE). [18]

Calibration curves of 4-NP. Concentration (c) dependences of 4-NP's peak current were measured by CV on a bPGE-AgAP (Figure 3). The extracted peak potential (E_p) and peak current (I_p) are presented in the inset graph and parameters of the calibration fit lines ($I_p = a \times c + b$) together with the limit of detection (LOD) are listed in Table 1. The LOD values were calculated using the following equations: LOD = 3.3×SD/a, where SD is the standard deviation of the intercept (b) and a is the slope of the calibration curve. [38]

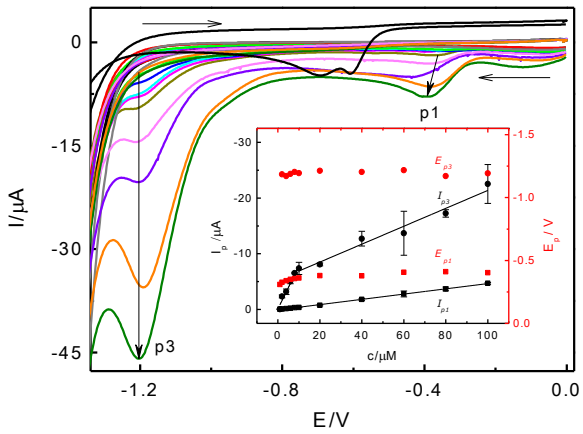

Figure 3. Cyclic voltammograms of 4-NP measured as a function of its concentration (0–100 µM) on a bPGE-AgAP. Extracted peak potentials (E_p) and heights (I_p) are shown in the inset (error bars correspond to ±standard deviation of 3 measurements). The black curve is cyclic voltammogram of 100 µM 4-NP measured on a bare bPGE in 0.2 M AcP pH 5.0 as a control.

Table 1. Parameters of the linear fit calibration lines of 4-NP using CV on bPGE-AgAP.

peak	a / µA µM^{-1}	b / µA	R^2	LOD / µM	c / µM
p1	−0.047 ± 0.048	0.075 ± 0.022	0.9991	1.5	1 - 100
p3	−0.777 ± 0.081	−0.06 ± 0.49	0.9582	2.1	1 - 10
p3	−0.163 ± 0.015	−5.29 ± 0.88	0.9684	-	10 - 100

Intensity (peak current) of the 4-NP´s p1 peak responds to its increasing concentration linearly within the concentration range from 1 to 100 µM at bPGE-AgAP. Obtained LOD 1.5 µM is comparable to values obtained by Fischer *et al.* using generally 10-times more sensitive differential pulse voltammetry (DPV) on the meniscus-modified silver solid amalgam electrode (1.1 µM) and/or polished silver solid amalgam electrode (2.8 µM). [39] Since a LOD 0.13 µM was reached by DPV at HMDE [24], analogical improvement in our LOD is expected using DPV or square-wave voltammetry, but developing an analytical method was not in the scope of this research. A broader comparison of the LOD values achievable by various voltammetric methods has already been summarized in Ref. [40].

3.4 Spectroelectrochemistry of 4-nitrophenol

Spectroelectrochemistry represents a simple yet powerful tool for simultaneous (on-line) registration of various optical signals and current/potential during ongoing electrochemical processes. Herein, potentiostatic electrolysis of 4-NP on bPGE-AgAP with simultaneous UV-Vis spectrometry was carried out to demonstrate its applicability in spectroelectrochemistry. To mitigate bPGE's low transparency, it has to be oriented in parallel to the light beam passing through the common 1 cm quartz cuvette (as reported in Ref. [20]).

The number of exchanged electrons during 4-NP electrolysis and corresponding reduction rate constants were determined for the selected applied potentials −0.6 V and −0.9 V. The applied potentials resulted from LSV registered before and after the electrolyses of 4-NP (100 µM) in 0.2 M AcP pH 5.0 (Figure 4A). Thanks to the simultaneous registration of the UV-Vis spectra (Figure 4C), accurate 4-NP concentration during electrolysis could be calculated using the Lambert-Beer law and then used to estimate the number of exchanged electrons using the Faraday law (Figure 4B and 4D, Table 2). The first-order reaction rate constants (k) corresponding to the slowest step of the electroreduction process could be evaluated from the slopes of the corresponding Equation 1:

$$\ln(c_{4\text{-NP}}) = k \times t + \ln c^0 \quad (1)$$

where k…rate constant, t…time, $c_{4\text{-NP}}$…4-NP concentration and c^0…initial 4-NP concentration (Table 2). About a 300 mV positive shift in the 4-NP cathodic peak observed on bPGE-AgAP, compared to the bare bPGE, indicates significant facilitation in the electrochemical reduction process. Four electrons consumed per one molecule of 4-NP, as assessed from our data, is in good agreement with the well-known mechanism of electrochemical reduction of aromatic nitro compounds. An applied potential of −0.6 V was sufficient to reduce 4-NP on the bPGE-AgAP, while −0.9 V had to be applied on the bare bPGE to reach equal reduction rate constants. Increasing the applied potential from −0.6 V to −0.9 V on the bPGE-AgAP speeded up 4-NP reduction from $4 \cdot 10^{-4}$ to $7 \cdot 10^{-4}$ mol L^{-1} s^{-1}, respectively.

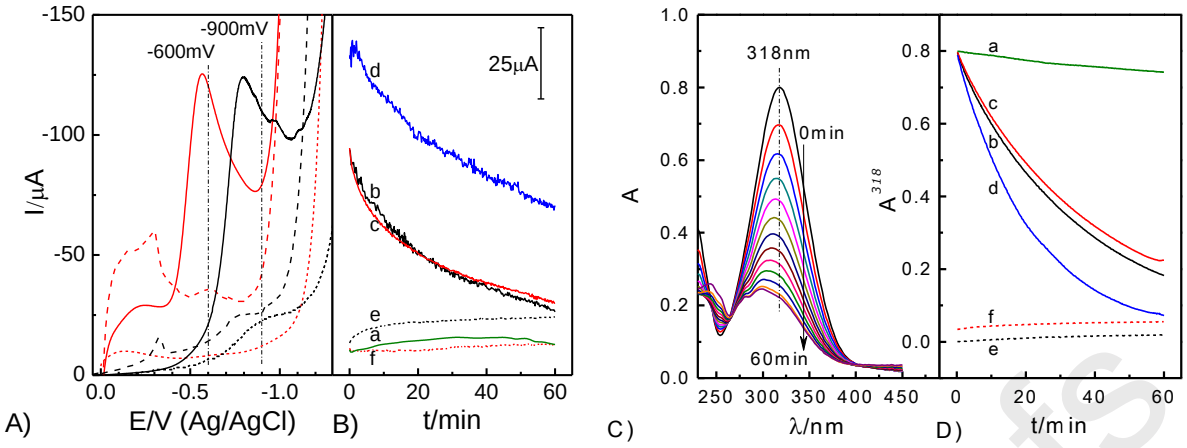

Figure 4. A) Linear scan voltammograms of 4-NP before (solid lines) and after its electrolysis (dash lines) on bPGE (black curves) with applied potential −0.9 V and on bPGE-AgAP (red curves) with applied potential −0.6 V in 0.2 M AcP pH 5.0 (short dash lines); B) chronoamperograms and D) extracted time-dependent absorbance at 318 nm of 4-NP registered on: bare bPGE at −0.6 V (a) and −0.9 V (b) and bPGE-AgAP using −0.6 V (c) and −0.9 V (d) and of 0.2 M AcP pH 5.0 (without 4-NP) on bare bPGE at −0.9 V (e) and on bPGE-AgAP at −0.6 V (f). C) UV-Vis spectra of 4-NP registered in 5-min intervals during chronopotentiometric electrolysis at bPGE-AgAP with the applied potential of −0.6 V. bPGE-AgAP prepared as mentioned in Fig. 3.

Table 2. Data obtained from the spectroelectrochemical study of 4-NP at 25±2°C.

Electrode/Applied potential	Number of electrons	Reaction order	k /mol L^{-1} s^{-1}
bPGE/ −600 mV	0	1st	$2 \cdot 10^{-5}$
bPGE/ −900 mV	4	1st	$4 \cdot 10^{-4}$
bPGE-AgAP/ −600 mV	4	1st	$4 \cdot 10^{-4}$
bPGE-AgAP/ −900 mV	4	1st	$7 \cdot 10^{-4}$

The 4-NP reduction kinetic has been studied for the first time in this work according to our best of knowledge. Obtained results proved the applicability of AgAPs in spectroelectrochemistry and intended optical studies, where absorption and reflectance of charged AgAPs will be studied in the presence or absence of adsorbed biopolymers (proteins and DNA). Moreover, our further studies will be focused to direct in-situ structural studies of biopolymers using spectroelectrochemistry including fluorescent microscopy, circular dichroism or Raman spectroscopy. Therefore, utilization of both techniques has been tested first separately.

3.5 Adsorption and detection of DNA and GFP on AgAP

Fluorescence microscopy. Adsorption of model biopolymers, such as fluorescently labelled calf thymus DNA and GFP, on the surface of bPGEs and ePGEs with or without electrodeposited AgAPs was observed by fluorescence microscopy (Figure 5a-h). Fluorescently labelled DNA showed remarkable fluorescence at the contour line around the co-localized AgAPs (compare panels (a) and (b) in Figure 5). Enhancing fluorescence around the particles, compared to the underlying bPGE, indicates preferential DNA adsorption at these sites. In the case of AgAPs electrodeposited on the ePGE, no significant difference in DNA adsorption was found (Figure 5d). On the contrary, microscope images 5f) and 5h) show significant GFP fluorescence only on AgAPs compared to bare bPGE or ePGE surfaces. Importantly, adsorbed protein's intense fluorescence also indicates the GFP native structure's preservation even after its interaction with the amalgam surface. The fact that the AgAP transducers do not influence the analyte structure is an important finding, which validates their further applications in electroanalysis and sensing. Due to low AgAP RSC on ePGE, the only bPGE was used in electrochemical studies.

Electrochemistry. Applicability of the bPGE-AgAP in electrochemical studies of DNA and proteins was investigated by AdTS techniques. Single-stranded ODN was used as a model DNA molecule. The ODN yielded a cathodic reduction peak of cytosine and adenine (CA peak) and an anodic oxidation peak of a guanine reduction product 7,8-dihydroguanine (G peak) at the bPGE-AgAP. These signals were analogous to those observed at the HMDE and were not detected on the bare bPGE under the given conditions (Figure 6). Dependences of CA and G peak heights on adsorption time of ODN, its concentration or constitution including the variable number of cytosines and guanines in the strands have also been registered using TSCV at bPGE-AgAP (Figures S8, S9, and S10 with related Table S2 and S3). In accordance with the expectation, CA and G peaks increased in heights with: i) prolonging adsorption time within 5 – 60 s for 10 ng μL^{-1} of ODN, ii) increasing ODN concentration within the range 1 – 10 ng μL^{-1} and iii) increasing number of cytosines and guanines in the ODN strands. These results are in good agreement with the theory [4] and could be utilized in direct DNA analysis or e.g. DNA/protein interaction studies.

As demonstrated above, GFP was preferentially adsorbed on the AgAPs electrodeposited on a PGE in both basal- and edge-plane orientations (Figure 5f and 5h). In the subsequent experiments, we tested the adsorbed GFP's electrocatalytic activity using AdTS constant current chronopotentiometry. 3 µM GFP yielded a well-developed peak H due to CHER [5] on the bPGE-AgAP, while no peak H was observed on the bare bPGE under the same conditions

(Figure 7A). The H peak's height was dependent on the GFP concentration — increasing up to 1 µM of GFP and levelling off at higher concentrations (Figure 7B). Notably, we have observed that even 100 nM GFP can be detected on the bPGE-AgAP with very good reproducibility (Figure 7C). The peak H corresponds to the electrochemical reduction of H^+ from protonated forms of basic moieties in the protein, which is adsorbed on the electrode surface and provides the catalytic reaction. Protons from the adsorbed protonated proteins are better accessible for their reduction, which thus proceeds at potential potentials less negative than hydrogen evolution occurring on the bare electrode. The reaction could be depicted by the following scheme adopted from the Ref. [41]:

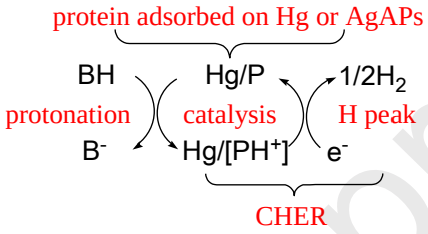

Since the peak H is provided by practically all proteins, it is not selective towards GFP. However, peak H allows a highly structure-sensitive analysis of proteins, including those important in biomedicine and cancer research [5]. Next to the mercury and polished or mercury meniscus-modified silver solid amalgam electrodes, bPGE-AgAP is the only one mechanically and chemically stable electrified interface providing protein sensitive peak H, which is moreover easy to miniaturize.

In summary, our results show that bPGE-AgAP could be used as a suitable alternative to HMDE in DNA and protein electroanalysis. [42] Detailed studies are in the scope of our further research and will be published elsewhere.

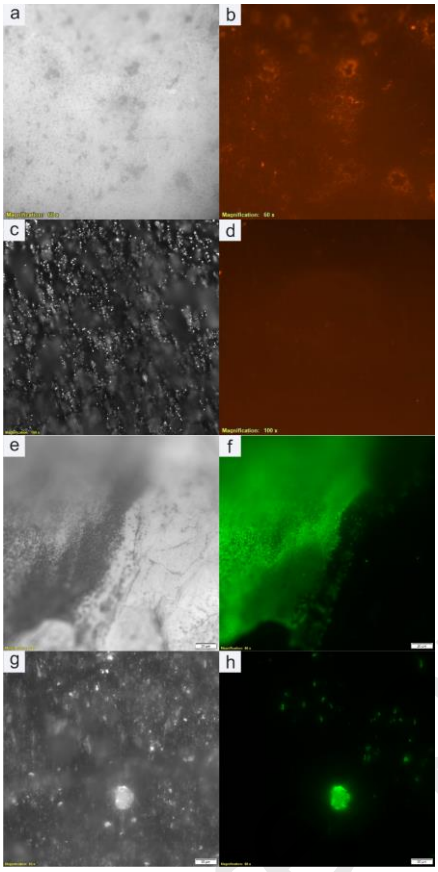

Figure 5. Microscope photographs of bPGE-AgAP (a, b, e, f) and ePGE-AgAP (c, d, g, h) with the adsorbed DNA (a, b, c, d) and GFP (e, f, g, h). The photographs capture: reflected light (a, c, e, g) and fluorescence at 560 nm (b, d) and 509 nm (f, h), (magnification 100×, view field 225 μm).

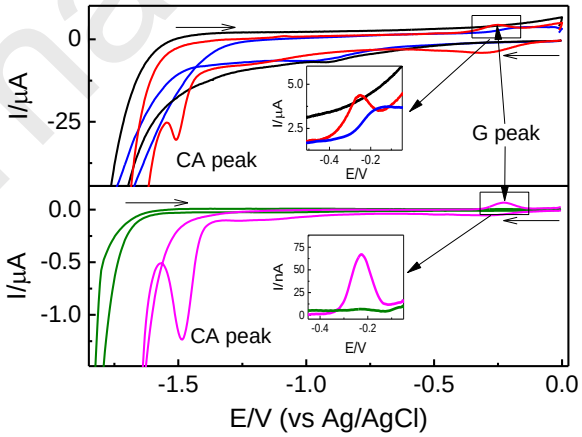

Figure 6. AdTS cyclic voltammograms of a model ODN on bPGE (top, blue curve), bPGE-AgAP (top, red curve) and a model ODN on HMDE (bottom, magenta curve) measured in 0.3 M AFP buffer pH 6.9 (top, black at bPGE-AgAP, and bottom, green at HMDE).

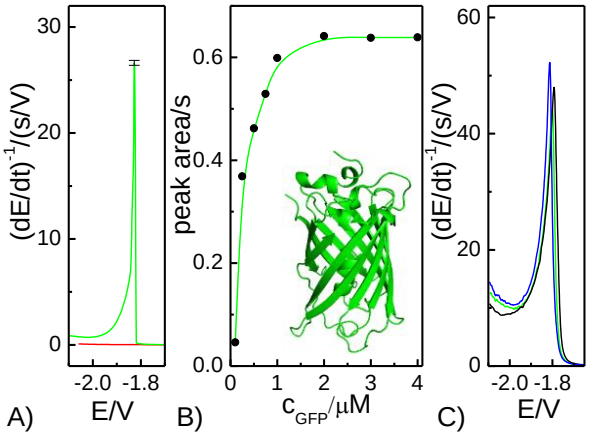

Figure 7. (A) AdTS chronopotentiograms of 3 μM GFP on bPGE (red) and bPGE-AgAP (green), I_{strip} = −300 μA. (B) Concentration dependence of the peak H area extracted from similar measurements to (A). The tertiary structure of the GFP is shown in the inset (GFP structure adopted from Ref. [43]). (C) Three-time repeated AdTS chronopotentiograms of 100 nM GFP on bPGE-AgAP, I_{strip} = −100 μA.

4. Conclusions and prospects

Electrochemical co-reduction of silver(I) and mercury(II) ions on the basal-plane pyrolytic graphite electrode from the solution was found to be a convenient procedure to prepare homogenous, sufficiently stable and mechanically robust AgAPs with controllable composition, particle size, distribution and surface coverage. The bPGE-AgAP's electrochemical properties were also studied by CV of an electrochemically reducible nitro compound, 4-nitrophenol. Voltammetric and spectroelectrochemical experiments with bPGE-AgAP demonstrated its applicability and perspectives in electroanalysis. In the context of bioelectroanalysis, adsorption of DNA and protein (GFP) was directly observed on the b/ePGE-AgAP by fluorescent microscopy. Thanks to the preferential adsorption of these biopolymers on AgAPs, the bPGE-AgAP proved to be applicable in their direct electroanalysis using voltammetry and constant current chronopotentiometry.

In general, AgAPs could be used as an alternative to the mercury electrodes, with prospective applications in detailed studies of biopolymers and of their structural changes on charged surfaces. Besides, our results suggest further applications in the development of various sensors, microfluidic and/or spectroelectrochemical cells applicable in *e.g.* Raman, plasmonics and/or spectroscopy of circular dichroism. In our opinion, AgAPs has a great potential for further (not only) biomedical applications employing direct analysis of biopolymers (nucleic acids, proteins, glycoproteins *etc.*) in basic research, early stage diagnostics, and/or treatment

(theranostics) of various disorders connected to DNA/protein damage or their structural changes.

Conflict of interest

There are no conflicts of interest to declare.

Acknowledgment

This work has been supported by the Grant Agency of the Czech Republic (project 17-23634Y) and by the SYMBIT project reg. no. CZ.02.1.01/0.0/0.0/15_003/0000477 financed from the ERDF. A part of this work was carried out with the support of CEITEC Nano Research Infrastructure (ID LM2015041, MEYS CR, 2016–2019), CEITEC Brno University of Technology.

Supporting Information Available: Effect of the w_{SOL} on the composition of electrodeposited AgA (Figure S1), SEM images together with evaluated effects of nucleation potential (E_1), growth potential (E_2) and time (t_2) (Figures S2 and S3) and cyclic voltammograms of 4-NP with evaluated peak currents (I_p) and potentials (E_p) in dependence on w_{SOL} (Figure S4 and S5), E_1, E_2, t_2 (Figure S6) and scan rate (Figure S7 and Table S1), voltammetry of ODNs in dependence on ODN adsorption time (Figure S8), concentration (Figure S9 and Table S2) and number of electroactive nucleobases (Figure S10 and Table S3) supports related data mentioned in the manuscript.

References

[1] Y. Zhai, Z. Zhu, S. Zhou, C. Zhu, S. Dong, Recent advances in spectroelectrochemistry, Nanoscale. 10 (2018) 3089–3111. doi:10.1039/c7nr07803j.

[2] E.T.S.G. da Silva, D.E.P. Souto, J.T.C. Barragan, J. de F. Giarola, A.C.M. de Moraes, L.T. Kubota, Electrochemical Biosensors in Point-of-Care Devices: Recent Advances and Future Trends, ChemElectroChem. 4 (2017) 778–794. doi:10.1002/celc.201600758.

[3] D. Hernandez-Santos, M.B. Gonzalez-Garcia, A.C. Garcia, Metal-nanoparticles based electroanalysis, Electroanalysis. 14 (2002) 1225–1235. doi:10.1002/1521-4109(200210)14:18<1225::AID-ELAN1225>3.0.CO;2-Z.

[4] E. Palecek, M. Bartosik, Electrochemistry of nucleic acids, Chem. Rev. 112 (2012) 3427–3481. doi:10.1021/cr200303p.

[5] E. Palecek, J. Tkac, M. Bartosik, T. Bertok, V. Ostatna, J. Palecek, Electrochemistry of nonconjugated proteins and glycoproteins. Toward sensors for biomedicine and glycomics, Chem. Rev. 115 (2015) 2045–2108. doi:10.1021/cr500279h.

[6] E. Palecek, M. Bartosik, Intrinsic Electrocatalysis in DNA, ChemElectroChem. 5 (2018) 936–942. doi:10.1002/celc.201700888.

[7] B. Yosypchuk, L. Novotny, Nontoxic Electrodes of Solid Amalgams, Crit. Rev. Anal. Chem. 32 (2002) 141–151. doi:10.1080/10408340290765498.

[8] B. Yosypchuk, J. Barek, Analytical Applications of Solid and Paste Amalgam Electrodes, Crit. Rev. Anal. Chem. 39 (2009) 189–203. doi:10.1080/10408340903011838.

[9] S. Hason, V. Vetterl, Detection of synthetic oligonucleotides by alternating current voltammetry at solid amalgam surfaces, Electrochim. Acta. 51 (2006) 5199–5205. doi:10.1016/j.electacta.2006.03.044.

[10] S. Hason, V. Vetterl, Microanalysis of oligodeoxynucleotides by cathodic stripping voltammetry at amalgam-alloy surfaces in the presence of copper ions, Talanta. 69 (2006) 572–580. doi:10.1016/j.talanta.2005.10.029.

[11] A. Danhel, V. Raindlova, L. Havran, J. Barek, M. Hocek, M. Fojta, Voltammetric Study of dsDNA Modified by Multi-redox Label Based on N-methyl-4-hydrazino-7-nitrobenzofurazan, Electrochim. Acta. 129 (2014) 348–357. doi:10.1016/j.electacta.2014.02.137.

[12] A. Danhel, V. Raindlova, L. Havran, H. Pivonkova, M. Hocek, M. Fojta, Electrochemical behaviour of 2,4-dinitrophenylhydrazi(o)ne as multi-redox centre DNA label at mercury meniscus modified silver solid amalgam electrode, Electrochim. Acta. 126 (2014) 122–131.

[13] R. Fadrna, B. Yosypchuk, M. Fojta, T. Navratil, L. Novotny, Voltammetric Determination of Adenine, Guanine, and DNA Using Liquid Mercury Free Polished Silver Solid Amalgam Electrode, Anal. Lett. 37 (2004) 399–413. doi:10.1081/AL-120028615.

[14] K. Kucharikova, L. Novotny, B. Yosypchuk, Detecting DNA damage with a silver solid amalgam electrode, 16 (2004). http://apps.isiknowledge.com/full_record.do?product=UA&search_mode=GeneralSearch&qid=1&SID=R1glWWvSuyXby5Lw9fQ&page=1&doc=8 (accessed October 21, 2015).

[15] B. Yosypchuk, M. Fojta, L. Havran, Voltammetric behavior of osmium-labeled DNA

at mercury meniscus-modified solid amalgam electrodes. Detecting DNA hybridization, Electroanalysis. 18 (2006) 186–194. http://apps.isiknowledge.com/full_record.do?product=UA&search_mode=GeneralSearch&qid=1&SID=R1glWWvSuyXby5Lw9fQ&page=1&doc=5 (accessed October 21, 2015).

[16] A. Danhel, B. Josypcuk, J. Barek, M. Fojta, B. Yosypchuk, J. Barek, M. Fojta, Possibilities and Prospects of Silver Amalgam in Electroanalytical Chemistry, Chem. List. 110 (2016) 215–221. http://www.chemicke-listy.cz/docs/full/2016_03_215-221.pdf.

[17] A. Saillard, Mercury Amalgam Electrodepositon on Metal Microelectrodes, Georgia Institute of Technology, 2005.

[18] A. Danhel, V. Mansfeldova, P. Janda, V. Vyskocil, J. Barek, Crystallic silver amalgam – a novel electrode material, Analyst. 136 (2011) 3656. doi:10.1039/c1an15342k.

[19] J. Tvrdikova, A. Danhel, J. Barek, V. Vyskocil, Voltammetric and amperometric determination of selected dinitronaphthalenes using single crystal silver amalgam based sensors, Electrochim. Acta. 73 (2012) 23–30. doi:10.1016/j.electacta.2011.09.074.

[20] A. Danhel, F. Ligmajer, T. Sikola, A. Walcarius, M. Fojta, Electrodeposition of silver amalgam particles on ITO - Towards novel electrode material, J. Electroanal. Chem. 821 (2018) 53–59. doi:10.1016/j.jelechem.2017.12.008.

[21] P. Havranova, F. Ligmajer, A. Danhel, Electrodeposition of Silver Amalgam on Thin Gold Film Electrodes for Voltammetric Detection of 4-Nitrophenol and DNA Labeled with Osmium Tetroxide-Bipyridine Complex, Electroanalysis. 31 (2019) 1952–1960. doi:10.1002/elan.201900306.

[22] F. Ligmajer, M. Horak, T. Sikola, M. Fojta, A. Danhel, Silver Amalgam Nanoparticles and Microparticles: A Novel Plasmonic Platform for Spectroelectrochemistry, J. Phys. Chem. C. 123 (2019) 16957–16964. doi:10.1021/acs.jpcc.9b04124.

[23] J. Spacek, A. Danhel, S. Hason, M. Fojta, Label-free detection of canonical DNA bases, uracil and 5-methylcytosine in DNA oligonucleotides using linear sweep voltammetry at a pyrolytic graphite electrode, Electrochem. Commun. 82 (2017) 34–38. doi:10.1016/j.elecom.2017.07.013.

[24] A. Niaz, J. Fischer, J. Barek, B. Yosypchuk, Sirajuddin, M.I. Bhanger, Voltammetric Determination of 4-Nitrophenol Using a Novel Type of Silver Amalgam Paste Electrode, Electroanalysis. 21 (2009) 1786–1791. doi:10.1002/elan.200904622.

[25] P. Vidlakova, H. Pivonkova, M. Fojta, L. Havran, Electrochemical behavior of

anthraquinone- and nitrophenyl-labeled deoxynucleoside triphosphates: a contribution to development of multipotential redox labeling of DNA, Monatshefte Fur Chemie. 146 (2015) 839–847. doi:10.1007/s00706-015-1435-6.

[26] ImageJ, 5.6.2015 (n.d.). http://rsb.info.nih.gov/ij/ (accessed October 10, 2017).

[27] O.S. Ivanova, F.P. Zamborini, Size-Dependent Electrochemical Oxidation of Silver Nanoparticles, J. Am. Chem. Soc. 132 (2010) 70–72. doi:10.1021/ja908780g.

[28] D. Tudela, Silver(II) Oxide or Silver(I,III) Oxide?, J. Chem. Educ. 85 (2008) 863. doi:10.1021/ed085p863.

[29] A. Milchev, E. Michailova, T. Zapryanova, Initial stages of electrochemical alloy formation: Size and composition of critical nuclei, Electrochem. Commun. 6 (2004) 713–718. doi:10.1016/j.elecom.2004.05.008.

[30] J. Galvez, M.L. Alcaraz, Y.B. Shim, S.M. Park, Double-potential-step chronoamperometry in the study of amalgam-forming and non-amalgam-forming systems at spherical electrodes (HMDE and DME). Analysis of the discrepancies between experimental results and theoretical predictions for amalgam formation, J. Electroanal. Chem. 341 (1992) 209–225. doi:10.1016/0022-0728(92)80485-M.

[31] M.R. Baren, The Ag-Hg (Silver-Mercury) system, J. Phase Equilibria. 17 (1996) 122–128. doi:10.1007/BF02665787.

[32] A. Danhel, B. Yosypchuk, V. Vyskocil, J. Zima, J. Barek, A novel paste electrode based on a silver solid amalgam and an organic pasting liquid, J. Electroanal. Chem. 656 (2011) 218–222. doi:10.1016/j.jelechem.2010.11.010.

[33] J. Tvrdikova, A. Danhel, V. Vyskocil, J. Barek, Voltammetric determination of dinitronaphthalenes using a silver solid amalgam paste electrode, Anal. Sci. 28 (2012). doi:10.2116/analsci.28.411.

[34] J. Tvrdikova, A. Danhel, J. Barek, VOLTAMMETRIC DETERMINATION OF DINITROPHENOLS AT A SILVER SOLID AMALGAM PASTE ELECTRODE, Chem. List. 104 (2010) S57–S60.

[35] A. Danhel, J. Barek, Solid amalgam electrodes in organic electrochemistry, Curr. Org. Chem. 15 (2011) 2957–2969. doi:10.2174/138527211798357218.

[36] T. Horibe, J. Zhang, M. Oyama, Effects of capping reagents on the electron transfer reactions on gold nanoparticle-attached indium tin oxide electrodes, Electroanalysis. 19 (2007) 847–852. doi:10.1002/elan.200603793.

[37] B. Dinesh, R. Saraswathi, Electrochemical synthesis of nanostructured copper-curcumin complex and its electrocatalytic application towards reduction of 4-

nitrophenol, Sensors Actuators B Chem. 253 (2017) 502–512. doi:10.1016/j.snb.2017.06.149.

[38] I.S. Krull, M.E. Swartz, Determining Limits of Detection and Quantitation, LC-GC Eur. 16 (1998) 922–924.

[39] J. Fischer, L. Vanourkova, A. Danhel, V. Vyskocil, K. Cizek, J. Barek, K. Peckova, B. Yosypchuk, T. Navratil, Voltammetric determination of nitrophenols at a silver solid amalgam electrode, Int. J. Electrochem. Sci. 2 (2007).

[40] R. Pfeifer, P. Tamiasso-Martinhon, C. Sousa, J.C. Moreira, M.A.C. Do Nascimento, J. Barek, Differential pulse voltammetric determination of 4-nitroaniline using a glassy carbon electrode: Comparative study between cathodic and anodic quantification, Monatshefte Fur Chemie. 147 (2016) 111–118. doi:10.1007/s00706-015-1596-3.

[41] T. Doneux, V. Ostatná, E. Paleček, On the mechanism of hydrogen evolution catalysis by proteins: A case study with bovine serum albumin, Electrochim. Acta. 56 (2011) 9337–9343. doi:10.1016/j.electacta.2011.08.017.

[42] E. Palecek, P. Boublikova, F. Jelen, Cyclic voltammetry of nucleic acids and determination of submicrogram quantities of deoxyribonucleic acids by adsorptive stripping voltammetry, Anal. Chim. Acta. 187 (1986) 99–107.

[43] Protein data bank, (n.d.). http://www.rcsb.org/pdb/results/results.do?tabtoshow=Current&qrid=75CBE431 (accessed March 11, 2019).

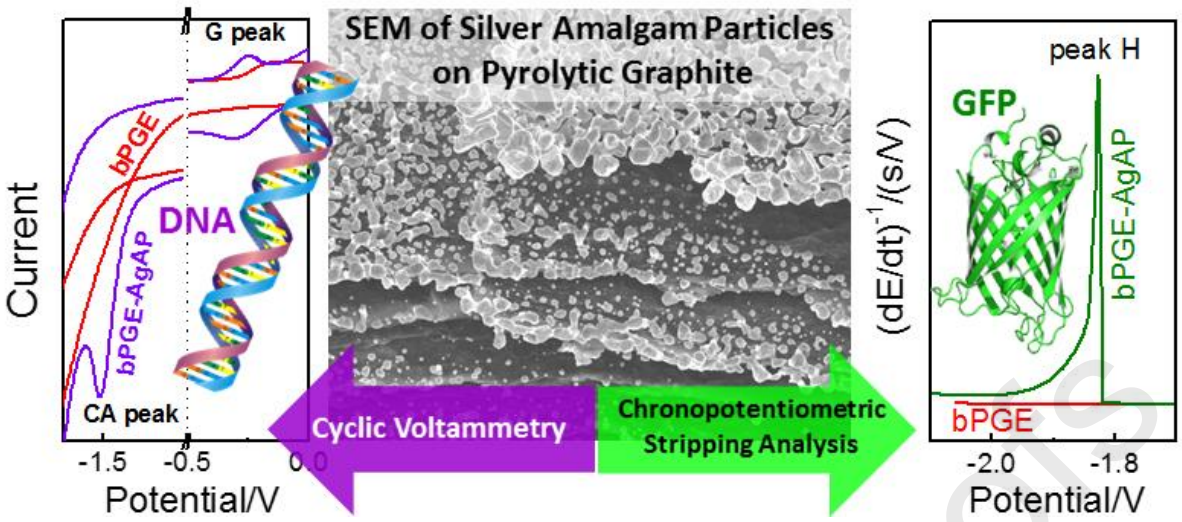

Highlights:

- Pyrolytic graphite allows electrodeposition of silver amalgam particles (AgAPs)
- AgAPs' constitution, morphology and distribution bPGE are adjustable
- bPGE-AgAP offers broad negative potential window for electrochemical studies
- DNA and GFP preferentially adsorb on AgAPs then on bPGE
- Intrinsic signals of DNA and chronopotentiometric peak H of GFP were detected